On the dynamic contact angle of capillarity-driven microflows in open channels

Jodie C. Tokihiro[a], Anika M. McManamen[a], David N. Phan[a], Sanitta Thongpang[a], Terence D. Blake[b], Ashleigh B. Theberge[a,c], Jean Berthier[a*]*

[a]*Department of Chemistry, University of Washington, Box 351700, Seattle, Washington 98195, United States*

[b]*Independent consultant, Tring, HP23 5JH, United Kingdom*

[c]*Department of Urology, University of Washington School of Medicine, Seattle, Washington 98105, United States*

[*]Co-corresponding authors: Jean Berthier, berthj2@uw.edu; Ashleigh B. Theberge, abt1@uw.edu

Phone: +1 206-685-2330 Fax: +1 206-685-8665

Abstract

The true value of the contact angle between a liquid and a solid is a thorny problem in capillary microfluidics. The Lucas-Washburn-Rideal (LWR) law assumes a constant contact angle during fluid penetration. However, recent experimental studies have shown lower liquid velocities than predicted by the LWR equation, which are attributed to a velocity-dependent dynamic contact angle that is larger than its static value. Inspection of fluid penetration in closed channels has confirmed that a dynamic angle is needed in the LWR equation.

In this work, the dynamic contact angle in an open channel configuration is investigated using experimental data obtained with a range of liquids, aqueous and organic, and a PMMA substrate. We demonstrate that a dynamic contact angle must be used to explain the early stages of fluid penetration, i.e., at the start of the viscous regime, when flow velocities are sufficiently high. Moreover, the open channel configuration, with its free surface, enhances the effect of the dynamic contact angle, making its inclusion even more important. We found that for the liquids in our study, the molecular-kinetic theory (MKT) is the most accurate in predicting the effect of the dynamic contact angle on liquid penetration in open channels.

Keywords: capillary flow, open-channel microfluidics, Lucas-Washburn-Rideal law, dynamic contact angle, molecular kinetic theory, viscous regime

1. Introduction

When a fluid flows in contact with a wall, its contact angle generally differs from its static value [1-3]. At the present time there are several approaches to predict the value of the dynamic contact angle (DCA) in the so-called viscous regime defined by Lucas, Washburn and Rideal (LWR) [4-6]: the hydrodynamic model (HD), the molecular kinetic theory (MKT) and empirical or semi-empirical correlations based on the capillary number. The basis for understanding the DCA has been established by, among others, de Gennes [7] who demonstrated that, for a partial wetting, the unbalanced interfacial tension forces $F = \gamma\,(cos\theta_0 - cos\theta_d)$— where γ is the liquid/air interfacial tension, θ_d and θ_0 are the dynamic and equilibrium contact angles respectively—must be compensated either by the viscous dissipation at a mesoscopic scale or by dissipation in the vicinity of the contact line or in the precursor film.

Abbreviations: LWR, Lucas-Washburn-Rideal law; PMMA, poly(methyl methacrylate); MKT, molecular kinetic theory; DCA, dynamic contact angle, HD, hydrodynamic model; TPCL, triple phase contact line; CAD, computer-aided design; CAM, computer-aided manufacturing; CNC, computer-numerical control; SLR, single lens reflective.

The hydrodynamic (HD) approach corresponds to the case of viscous dissipation at the mesoscopic scale resulting in so-called viscous bending near the wall (Figure 1A) [8-11].

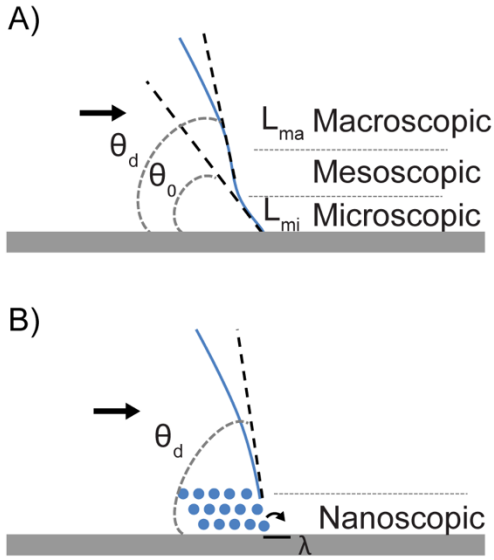

Figure 1. Sketches of the two main models for DCA: A, the hydrodynamic model (HD) assuming a viscous bending at the wall; B, the molecular dynamic theory (MKT) with the rolling motion of molecules at the wall.

In the HD approach, the increase jn the contact angle outside of the microscopic region (L_{mi}) is linked to the cubic root of the capillary number [8]

$$\theta_d^3 = \theta_0^3 + 9\,\chi Ca = \theta_0^3 + 9\,ln(L_{ma}/L_{mi})\,Ca\,, \quad (1)$$

where Ca is the capillary number ($Ca = \mu V/\gamma$, μ being the fluid viscosity and γ the fluid surface tension) and χ is a parameter given by $\chi = ln(L_{ma}/L_{mi})$, L_{ma} being a macroscopic length scale which is of the order of the size of the meniscus and L_{mi} a microscopic length scale, which is the cutoff length below which the continuum theory breaks down.

On the other hand, adsorption-desorption dynamics of liquid molecules on a solid surface near the TPCL (triple phase contact line) is the basis for the molecular kinetic theory (MKT, Figure 1B). This approach was first proposed by Blake and Haynes [12] using Eyring's activated-rate theory of stress-modified activated rate processes [13]. According to the MKT, to an approximation, the velocity-dependent dynamic contact angle is given by [12,14,15]

$$\Delta F_{cap} = \gamma\,(cos\theta_d - cos\theta_0) = -\zeta\,V, \quad (2)$$

where ζ is the coefficient of contact line friction per unit length of the contact line (unit Pa.s). The other parameters have already been defined. Strictly speaking, this simple linear form applies only near equilibrium or where the energy barriers to contact-line movement are small; but as we are interested only in the way in which a change in the dynamic contact angle may provide a correction to the viscosity-dominated flow in the channel, this form is adequate for our immediate purposes.

It was later demonstrated [14-17] that the contact-line friction is related to the equilibrium work of adhesion, Wa, by

$$\frac{\zeta}{\mu} \cong \frac{V_m}{\lambda^3}\exp\left(\frac{W_a}{n\,k_B T}\right) \cong \frac{V_m}{\lambda^3}\exp\left(\frac{\lambda^2 W_a}{k_B T}\right) \quad (3)$$

where λ is the characteristic distance of each molecular displacement (Figure 1B), k_B is the Boltzmann constant, T the temperature (in Kelvin), V_m is the molecular flow volume of the liquid, here approximated by the molecular volume. In (3), n is the number of solid-liquid interaction sites per unit area of the solid surface, provided these are distributed uniformly, $n \cong 1/\lambda^2$.

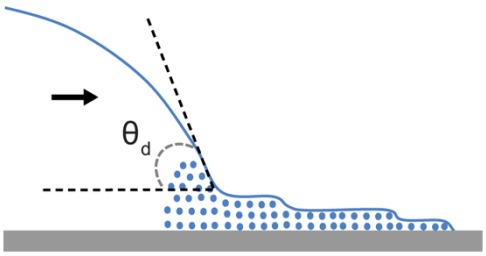

Figure 2. Sketch of the molecular kinetic theory – self layering approach where the precursor film is composed of layers of fluid molecules (represented as blue circles).

Note that, in the specific case of the existence of a precursor film [18,19] (where a thin sheet of fluid precedes the triple point contact line), a modified approach of MKT—called MKT-self-layering—assumes the formation of layers of molecules in the precursor film at the wall combined with the adsorption-desorption phenomenon (Figure 2) [20-22]. In this model, the wall viscosity, β, is then given by

$$cos\theta_d - cos\theta_0 = -\beta\, V, \qquad (4)$$

with $\frac{\beta}{\mu} = \exp\left(\frac{2\,\gamma}{n\,k_B T}\right)$, where μ is the viscosity of the flowing liquid, and n is the number of molecules per unit area in the precursor thin film, which is related to σ or the effective diameter of the molecules in the thin film by $n = 1/\sigma^2$.

Finally, let us remark that empirical and semi-empirical correlations have been proposed to predict the value of the DCA. These correlations make use of the capillary number and have the form [23-28]

$$cos\theta = cos\theta_0 - A(1 + cos\theta_0)\, f(Ca)\,, \qquad (5)$$

Where A is a non-dimensional coefficient and f is a monotonously increasing function. In many of these correlations, the function, f, is of the form, $f(Ca) = ACa^B$, where Ca is the capillary number, A is a correlation constant (ranging between 2 and 4.96), and B is a constant (ranging between 0.42 and 0.7). The term $1 + cos\theta_0$ represents the adhesion energy, $Wa = \gamma\,(1 + cos\theta_0)$.

In this work, we focus on the dynamic contact angle in capillary flows in open channels [29-31]. Contrary to traditional closed channel microfluidics, open channels are characterized by one or more air-liquid interfaces through the removal of at least one channel wall. Open channels have recently gained attention in the microfluidics community due to advantages such as accessibility, easy fabrication or surface treatment of the microfluidic channels, and the reduction in bubble formation during fluid addition and flow. These devices are simple to operate, necessitating only a micropipette, fluid of choice, and the open channel device. Open microfluidics has become widely used in a variety of research fields such as cell culture, protein and metabolite assays, organ-on-a-chip models, and even space applications [32-35]. To some extent, the physics of the microflow in open channels resembles that in closed channels, but some considerations must be adopted for open-channel flow. The LWR law must be modified by using an equivalent contact angle [30,31]—the so-called generalized Cassie angle–in place of the contact angle, and an average friction length in place of the tube radius.

It is shown here that, in the early stages of the viscous regime, a dynamic contact angle (DCA) should be used and, based on our experiments, that the most accurate approach is the molecular kinetic model. Our study employs rectangular open-channels milled in poly(methyl methacrylate) (PMMA)—slightly rounded at the bottom inner corners to avoid capillary filaments [36], and several different liquids including water, nonanol, pentanol, chloroform, FC-40, and an aqueous solution of 50% (v/v) isopropyl alcohol.

2. Materials and methods

a. *Channel Design and Fabrication*

Four different open rectangular channels milled in PMMA have been used: channel #1 (w = 1 mm, h = 2 mm), channel #2 (w = 2 mm, h = 2mm), channel #3 (w = 0.4 mm, h = 0.6 mm), and channel #4 (w = 0.4 mm, h = 0.4

mm). An engineering drawing of channel #1 is shown in Figure 3. Detailed engineering drawings of channels #1-4 can be found in Figure S1.1.1. Calibration markers separated by a known distance apart were milled into the device for scaling purposes during image analysis (Figure 3B). A profilometer photo of the rounded corners is shown in Figure 3B.

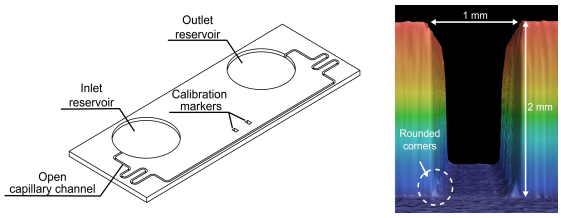

Figure 3. A: Isometric view of channel #1 milled in PMMA and **B:** profilometer cross-section of the channel with the rounded corners.

The characteristics of the channels are listed in Table 1.

Table 1. Characteristics of the channels

Channel	Width	Height	Max channel length	Wetted perimeter	Free perimeter	Friction length
Symbol *units*	*w [mm]*	*h [mm]*	*l* *[mm]*	p_W *[mm]*	P_F *[mm]*	$\bar{\lambda}$ *[mm]*
Channel #1	1.0	2.0	303	5.0	1.0	0.22
Channel #2	2.0	2.0	120	6.0	2.0	0.44
Channel #3	0.40	0.60	110	1.6	0.4	0.09
Channel #4	0.40	0.40	110	1.2	0.4	0.07

The average friction lengths (rightmost column in Table 1) representing the wall friction are first approximated by either of the semi-empirical formulations [30,37,38] either:

$$\bar{\lambda} \cong \frac{1}{3}\frac{w+h}{\left(\frac{2h}{w}+\frac{w}{h}\right)}, \qquad (6)$$

or

$$\bar{\lambda} \cong \frac{2}{3}\frac{h}{w}\chi\left(\frac{h}{w}\right)(w+h), \qquad (7)$$

where $\chi\left(\frac{h}{w}\right) = 1 + 0.671\frac{h}{w} + 4.1697\left(\frac{h}{w}\right)^2$.

These two formulas produce approximate values of the friction length for moderate aspect ratio rectangular open channels. The values are then adjusted on the experimental plots for the flow velocity, using velocities far from the channel entrance, where the contact angle most resembles the static contact angle—as will be shown later in the text (Figure 4).

The channels were designed using a computer-aided design (CAD) software (Solidworks 2017, Waltham, MA) and the design files were converted to a .simpl file using a computer-aided manufacturing (CAM) software (Fusion 360, Autodesk, San Rafael, CA). Channels were milled in PMMA sheets (3.175 mm thick, #8560K239; McMaster-Carr, Sante Fe Springs, CA).

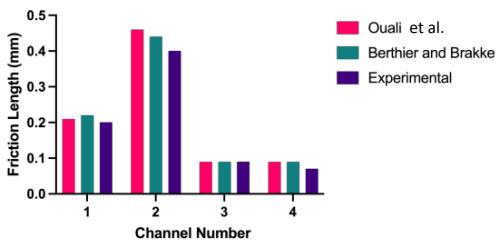

Figure 4. Comparison of the different approaches for the friction length: Ouali et al. [38] (pink color); Berthier and Brakke [37] (teal color); experiments (dark blue color).

To create round bottom channels, endmills with a cutter diameter of 1/32" (TR-2-0312-BN) or 1/64" (TR-2-0150-BN) were used (Performance Micro Tool, Janesville, WI). The devices were fabricated via micro-milling on a Datron Neo computer numerical control (CNC) mill (Datron, Germany). After fabrication, the channel dimensions were confirmed using a Keyence wide-area 3D measurement VR-5000 (Keyence Corporation of America, Itasca, IL). The channel bottom is estimated to have a few microns of roughness—due to the milling process— which is one magnitude below the roughness values observed by Lade *et al.* to produce substantial fluctuations in velocity [39]. Note that the effect of small roughness on open-capillary flow dynamics is not yet completely understood, since small reliefs on the wall surface slightly increase the capillary force —due to the Wenzel effect [40]—but also slightly increase the friction force [41]. In our case, the adjustment of the friction length indirectly takes this effect into account.

b. Solvent Prep and Physical Properties

Various solvents have been used in this study. Aqueous solvents included: deionized and distilled water (American Society for Testing and Materials Type II, HARLECO, Sigma-Aldrich, St. Louis, MO) as well as isopropyl alcohol at a concentration of 50% (v/v) in deionized and distilled water. These solvents were colored with 0.60 % yellow or 1.2 % blue food coloring. (McCormick). Organic compounds such as nonanol (Sigma-Aldrich, St. Louis, MO), pentanol (Sigma-Aldrich, St. Louis, MO), and chloroform (Fisher Scientific, Hampton, NH) have been colored with either Solvent Yellow 7 or with Solvent Green 3 (Sigma-Aldrich, St. Louis, MO) at concentrations of 0.50 mg/mL and 1.43 mg/mL respectively. FC-40 (Sigma-Aldrich, St. Louis, MO) was not colored, but tracking its travel in the channel was still feasible. In the case of water, the channel was treated by oxygen plasma using a Diener Zepto PC EX Type PB plasma treater (Diener Electronic, Germany) no more than 30 minutes prior to experimentation, to avoid contact angle relaxation.[23]
[42,43].

The physical data for these liquids are listed in table 2.

Table 2. Properties of the liquids

	γ [mN/m]	μ [mPa.s]	θ	w [mm]	h [mm]	cos θ*
Water	72	1.0	46	0.4	0.6	0.30
Chloroform	28	0.6	15	1	2	0.64
50% (v/v) Isopropyl alcohol	30	3.0	18	0.4	0.4	0.46
50% (v/v) Isopropyl alcohol	30	3.0	18	1	2	0.63
50% (v/v) Isopropyl alcohol	30	3.0	18	2	2	0.46
FC-40	16	2.5	17	1	2	0.63
Pentanol	25	3.7	13	2	2	0.48
Nonanol	27	11.5	13	2	2	0.48

*Note: These values are from Mohammad *et al.* 2014[24] and Kim *et al.* 2016[25]

The values of the physical properties of the liquids have been taken from physical tables and the literature [44,45], and the contact angles with PMMA have been measured in [46]. The generalized Cassie angle $\theta*$ is defined by:

$$cos\theta^* = \frac{p_W}{p} cos\theta_0 - \frac{p_F}{p}, \qquad (8)$$

where θ_0 is the Young (static) contact angle, p_W and p_F are the wetted and free perimeters in a cross section, and $p = p_W + p_F$. In the present case, setting the cross section to a rectangle of width, *w,* and height, *h:*

$$cos\theta^* = \frac{(w+2h)cos\theta_0 - w}{2\,(w+h)}. \qquad (9)$$

c. Open-Channel Flow Experiments

To obtain fluid velocities, the prepared fluids were flowed through the uniform cross section channels (#1-4). In channel #1, 2.2 mL of the dyed chloroform, water, and the colorless FC-40 were added to the inlet reservoirs of individual devices. For the devices using chloroform and water, which required an extended travel distance, a refill of 300 µL of the flowing fluid was added to the inlet reservoir to minimize the effect of pressure on the fluid dynamics. A refill was not added for FC-40, since data collection stopped after the fluid front reached the first calibration marker. Data were collected for the chloroform and water experiments until the fluid front of each

respective device reached the outlet reservoir. For channel #2, 2.2 mL of the dyed 50% (v/v) isopropyl alcohol, nonanol, and pentanol were added to the inlet reservoir of individual devices connected to the cross section corresponding to w = 2 mm and h = 2 mm. Data were collected until the fluid surpassed the first calibration maker. For channel #3, 140 µL of the dyed water was added to the plasma treated device and data were collected until the fluid front reached the outlet reservoir. For channel #4, 170 µL of 50% isopropyl alcohol was added to the inlet reservoir and data were collected until the fluid front reached the outlet reservoir. For each fluid in each channel dimension, experiments were completed in triplicate (n = 3) was used.

Videos of the progression of the flow of the solvent in the device were recorded using a Nikon-D5300 ultra-high resolution single lens reflective (SLR) camera at 60 fps. A video frame was analyzed every 10 frames using an execution file written in Python (execution file provided in SI). The distance that the fluid front had traveled was measured using ImageJ. The scale for each trial was set using the "Set Scale" function and the calibration markers on the device. The fluid front was tracked using the segmented line function and the total travel distance for each frame was measured using the "Measure" function. Data were exported as a .csv file and imported into Microsoft Excel. Calculations for fluid velocity and comparisons to the theoretical model were also conducted in Microsoft Excel.

3. Theoretical approach

Using the geometry of the open channel, the LWR law yields the relation between velocity, *V,* and travel distance, *z,*

$$V = \frac{\gamma}{\mu}\frac{\bar{\lambda}cos\theta^*}{z}, \qquad (10)$$

where $\bar{\lambda}$ is the average friction length which describes the wall friction, θ^* is the generalized Cassie angle which accounts for the effect of the free surface, γ is the surface tension of the liquid, and μ is the viscosity. Relation (10) can be rewritten in terms of the capillary number (*Ca*):

$$Ca = \frac{\mu}{\gamma}V = \frac{\bar{\lambda}cos\theta^*}{z} \ . \qquad (11)$$

Here, the DCA depends on the value of the velocity, represented by the capillary number. Relation (11) shows that if the travel distance is sufficient and/or the channel cross section is sufficiently small ($\bar{\lambda}/z \ll 1$), the use of the static contact angle is justified. Conversely, if this condition is not met, a DCA is present and changes the dynamics of the flow.

In this section, it is shown that the MKT approach can be applied analytically, leading to an easy modification of the extended LW law to take into account the dynamic contact angle. This observation was also made by Wu *et al.* [22] for capillary rise, using the LWR law with an equivalent radius.

In the viscous regime, the capillary force (F_{cap}) balances the wall friction force (whether the channel is closed or open), and

$$F_{cap} = p\,\gamma cos\theta^* = F_{drag} = p\,z\,\mu\frac{V}{\bar{\lambda}}. \qquad (12)$$

In relation (12), *z* is the marching—or travel—distance, *p* is the total perimeter of a cross section (including the liquid/air boundary if any), $\bar{\lambda}$ is the average friction length [30], and θ^* is the generalized Cassie angle [47]. Substituting $V = dz/dt$, relation (12) can be written as

$$zV = \frac{1}{2}\frac{dz^2}{dt} = \frac{\gamma}{\mu}\bar{\lambda}\,cos\theta^* \ , \qquad (13)$$

or

$$z^2 = \frac{\gamma}{\mu}2\bar{\lambda}\int_0^t cos\theta^* dt \ , \qquad (14)$$

In the case where θ^* is constant, the usual extended Lucas-Washburn law is retrieved. Using the expression of the generalized Cassie angle (8), relation (14) becomes

$$z^2 = \frac{\gamma}{\mu} 2\bar{\lambda} \int_0^t \left(\frac{p_W}{p} cos\theta - \frac{p_F}{p}\right) dt \,. \qquad (15)$$

Now, let us use the MKT correlation (4) to express the dynamic contact angle

$$z^2 = \frac{\gamma}{\mu} 2\bar{\lambda} \int_0^t \left[\frac{p_W}{p}\left(cos\theta_0 - \frac{\zeta}{\gamma} V\right) - \frac{p_F}{p}\right] dt = \frac{\gamma}{\mu} 2\bar{\lambda} \int_0^t \left[\left(\frac{p_W}{p} cos\theta_0 - \frac{p_F}{p}\right) - \frac{p_W}{p}\frac{\zeta}{\gamma}\frac{dz}{dt}\right] dt \,, \qquad (16)$$

or

$$z^2 = \frac{\gamma}{\mu} 2\bar{\lambda}\, cos\theta_0^* t - \frac{\gamma}{\mu} 2\bar{\lambda} \int_0^t \frac{p_W}{p}\frac{\zeta}{\gamma}\frac{dz}{dt} dt \,. \qquad (17)$$

The first term in (17) is the travel distance using the static contact angle ($z_0^2 = \frac{\gamma}{\mu} 2\bar{\lambda}\, cos\theta_0^* t$), and the second term is a correction due to the dynamic contact angle. Relation (17) can be simplified as

$$z^2 = \frac{\gamma}{\mu} 2\bar{\lambda}\, cos\theta_0^* t - 2\bar{\lambda}\frac{p_W}{p}\frac{\zeta}{\mu} z \,. \qquad (18)$$

The real travel distance—accounting for the dynamic contact angle correction—is then solved using the quadratic equation:

$$z^2 + 2\bar{\lambda}\frac{p_W}{p}\frac{\zeta}{\mu} z - z_0^2 = 0 \,. \qquad (19)$$

In (19), we must keep in mind that z and z_0 are functions of the time, t. Therefore, we finally obtain:

$$z = -\bar{\lambda}\frac{p_W}{p}\frac{\zeta}{\mu} + \sqrt{\left(\bar{\lambda}\frac{p_W}{p}\frac{\zeta}{\mu}\right)^2 + z_0^2} \,. \qquad (20)$$

It is verified that at $t = 0$ (we neglect the evanescent inertial motion [48]), $z_0 = 0$ and $z = 0$. For a long channel, z_0 becomes large and $z \rightarrow z_0$.

Flow velocity can be easily deduced from (20) by time differentiation:

$$V = \frac{V_0}{\sqrt{1 + \frac{\left(\bar{\lambda}\frac{p_W}{p}\frac{\zeta}{\mu}\right)^2}{z_0^2}}} \,, \qquad (21)$$

where V_0 is the velocity obtained using the static contact angle, $V_0 = dz_0/dt$. When the travel distance increases, z_0 increases and the real velocity V converges towards the velocity, V_0. Note that when z_0 goes to zero, z goes to zero, and relation (21) indicates that V goes to $V(z \rightarrow 0) = V_0 z_0 / \bar{\lambda}\frac{p_W}{p}\frac{\zeta}{\mu} = p\,\gamma cos\theta^* / \zeta p_W$, indicating that ζ acts like a viscosity associated with the triple line. However, in reality, relation (21) holds when the inertial regime ends i.e., when $z_0 > z_{inertial}$.

4. Experimental results and comparison with model

The importance of the DCA is directly linked to the velocity of the flow. As the flow velocity in the channel is proportional to the ratio of the surface tension and viscosity $V \approx (\gamma/\mu)/z$, we have categorized the fluids as "fast" and "slow" as a function of their intrinsic velocity, $V_i = \gamma/\mu$. The "fast" fluids correspond to high values of V_i ($V_i \gtrsim 30\ m/s$) and "slow" fluids by low values of V_i ($V_i \lesssim 8\ m/s$).

Water and chloroform are in the first category. Figure 5 shows the dynamics of these two fluids in channels of different cross sections. Clearly, the LWR law which uses the static (Young) contact angle does not account for the flow velocity. A DCA is required to fit the experimental results as seen in Figure 5 where the experimental

travel distances and velocities are closely fitted to the values predicted by the DCA theory (blue line). This DCA is obtained using ζ= 0.32 Pa.s for water and 0.20 Pa.s for chloroform.

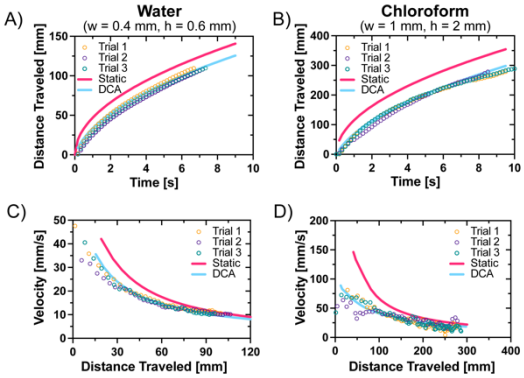

Figure 5. Comparison of models using the static and dynamic angles. Plots of travel distance vs. time for water in channel #3 (w = 0.4 mm, h = 0.6 mm) (**A**) and chloroform in channel #1 (w = 1 mm; h = 2mm) (**B**): comparison between the static contact angle (pink line), dynamic contact angle model (blue line) and experiments (circles). Plots of velocity vs. travel distance for water (**C**) and chloroform (**D**): comparison between the static contact angle model (pink line), dynamic contact angle model (blue line), and experiments (circles).

The solution of 50% (v/v) isopropyl alcohol in water is located in the "intermediate" fluids, categorized by a moderate $V_i = \gamma/\mu$ value. Figure 6 shows the dynamics of the flow in relatively large channels (w = 1 mm, h = 2 mm) (Figure 6A and C) compared to small cross sections (w = 0.4 mm, h = 0.4 mm) (Figure 6B and D).

In the first case, where a large cross section was used, a DCA is needed to account for the dynamics as shown through the experimental data clustering around the theoretical DCA travel distances and velocities (Figure 6A and C). On the other hand, the static angle (pink line) is sufficient in the second case of small cross sections (Figure 6B and D). The explanation is related to the value of the velocities, which are high in the first case, and small in the second case.

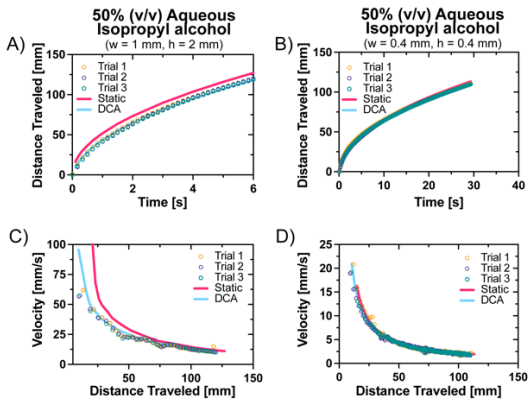

Figure 6. Comparison of models using the static and dynamic angles. Plots for travel distance vs. time for 50% (v/v) aqueous isopropyl alcohol in channel #1 (w = 1 mm, h = 2 mm) (**A**) and in channel #4 (w = 0.4 mm; h = 0.4 mm) (**B**): comparison between the static contact angle model (pink line), dynamic contact angle model (blue line), and experiments (circles). Plots of velocity vs. travel distance for 50% isopropyl alcohol in channel #1 (w = 1 mm, h = 2 mm) (**C**) and in channel #4 (w = 0.4 mm; h = 0.4 mm) (**D**): comparison between the static contact angle model (pink line), dynamic contact angle model (blue line), and experiments (circles).

In the last case of "slow" fluids, the preceding observation is still valid. Figure 7 shows a comparison of the dynamics of pentanol and nonanol in large channels (w = 2 mm, h = 2mm) for which the wall friction is minimal. A DCA is needed in the case of pentanol (V_i~7 m/s) (Figure 7A and C), but it is not needed for the case for nonanol (V_i~2.5 m/s) (Figure 7B and D).

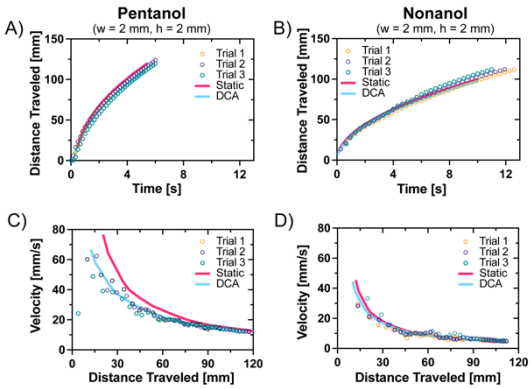

Figure 7. Comparison of models using the static and dynamic angles. Plots of travel distance vs. time for pentanol (**A**) and nonanol (**B**) in channel #2 (w = 2 mm, h = 2 mm): comparison between the static contact angle model (orange line), dynamic contact angle model (purple line), and experiments (dots). Plots of velocity vs. distance for pentanol (**C**) and nonanol (**D**): comparison between the static contact angle model (pink line), dynamic contact angle model (blue line), and experiments (circles).

5. Comparison with other correlations

In this section, we briefly present other correlations for DCA and compare them to the MKT approach used in section 3.

Hydrodynamic correlation proposed by Hoffman and Tanner [23,24] yields

$$\theta = 4.5\ Ca^{\frac{1}{3}}\,. \qquad (22)$$

Bracke *et al.* correlation [26,27] links the cosine of the dynamic contact angle to the capillary number:

$$cos\theta = cos\theta_0 - 2(1 + cos\theta_0)\ Ca\,. \qquad (23)$$

This correlation is very similar to the Seebergh and Berg [28] correlation, while the Jiang *et al.* correlation [25] yields:

$$cos\theta = cos\theta_0 - (1 + cos\theta_0)\ 4.96\ \tanh\left(Ca^{0.702}\right)\,. \qquad (24)$$

In order to investigate the effectiveness of these empirical correlations to account for the influence of a dynamic contact angle in the LWR equation, a numerical scheme was set up in a Matlab file [50] for each correlation. A comparison of the different correlations is shown in Figure 8A for water flowing in the channel #3 (w = 0.4 mm, h = 0.6 mm). Comparison for chloroform and 50% (v/v) isopropyl alcohol are shown in SI.1.

The evolution of the DCA with the distance is plotted in Figure 8A for the capillary flow of water in channels of cross section, w = 0.4 mm and h = 0.6 mm. The different approaches—constant static contact angle, HD correlations, and MKT—are compared. The MKT approach is the only one that fits the experimental data.

The generalized DCA given by its cosine,

$$cos\theta_d^* = \frac{p_W}{p} cos\theta_d - \frac{p_F}{p}, \qquad (25)$$

depends on the capillary number and is shown in Figure 8B (the value at *Ca* = 0 corresponds to the static Young angle) for the different correlations (Bracke *et al.*, Jiang *et al.*, Hoffman, MKT) using the data for water. The results are very similar except for the MKT correlation with a coefficient ζ = 0.35 Pa.s.

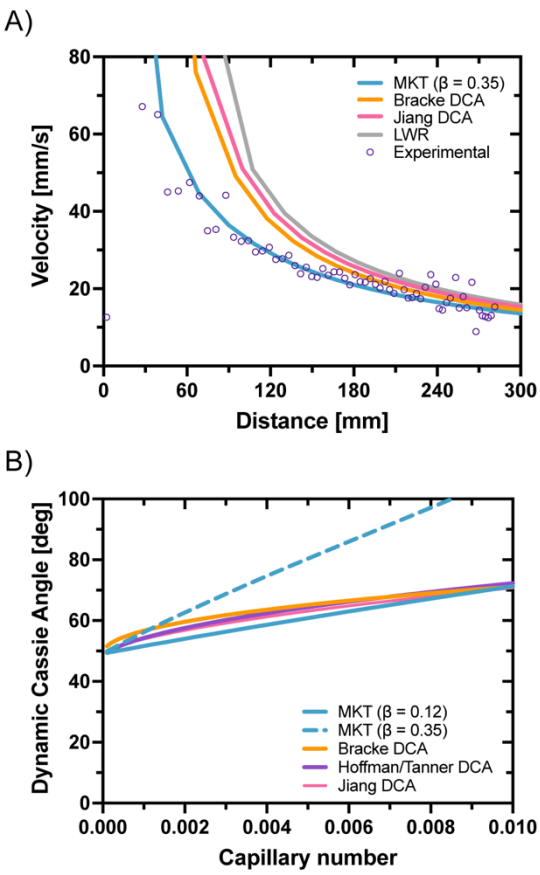

Figure 8. A: Comparison of the velocity of a water flow in the channel #3 between experiments (open circles), and different correlations; **B:** Comparison between the dynamic contact angles (Cassie generalized contact angles) obtained using the different correlations described in the text in function of the capillary number. The two blue lines corresponds to MKT correlations for ζ = 0.12 (Blue line) and 0.35 Pa.s (blue dotted line).

In Figure 9A and B, the relations between the DCA and the velocity and between the DCA and the travel distance, respectively, are shown for the different liquids used in this work. The importance of taking into account a DCA is evident for the first 50 mm of the open channels.

6. Discussion

Let us first remark that the advantage of using an open-channel configuration to assess the MKT approach is the increased sensitivity of the flow velocity to the DCA. A correction, ε, to the cosine of the contact angle has a stronger influence on the capillary force in the case of an open flow:

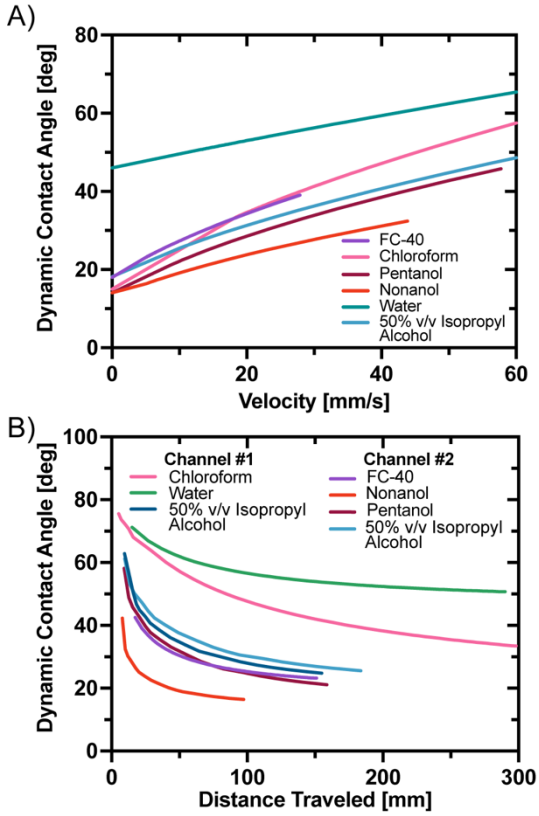

Figure 9. A: DCA vs. velocity for the 6 liquids (in the case of water, the PMMA has been treated with O_2 plasma) and **B:** evolution of the DCA with the distance in the channel for in different cases investigated in this work.

$$\frac{\Delta F_{cap}}{F_{cap}}(open) = \frac{(cos\theta_0^* - \varepsilon)}{cos\theta_0^*} = 1 - \frac{\varepsilon}{(p_W/p)\, cos\theta_0 - p_F/p}, \quad (26)$$

compared to

$$\frac{\Delta F_{cap}}{F_{cap}}(closed) = 1 - \frac{\varepsilon}{cos\theta_0}. \quad (27)$$

The sensitivity of an open microflow in a rectangular channel has recently been pointed out by Chang *et al.* [48].

A second remark is focused on the flow regimes (inertial or viscous). In the inertial regime, the velocity field is not established [49]; even if there is the effect due to the triple line friction on the contact angle, the different models presented here cannot be used. We verify that the experimental results used in this work correspond to the viscous regime. In Figure SI.2.1, the transition times and distances for the liquids and channels used in this study are calculated and listed. It is checked that the corrections associated with ζ shown in Figures 5, 6, and 7 correspond to the viscous regime and not the inertial regime. In Table 3, the inertial-viscous transitions for the different cases of Figures 5, 6, and 7 are listed. These times (t_{in}) and travel distance (z_{in}) transitions are located at the very beginning of the velocity vs. distance plots and do not interfere with the MKT approach (and other approaches).

Table 3. Transition data between inertial and viscous regimes

	Channel	Liquid	t_{in} [ms]	z_{in} [mm]
Figure 5				
	#3	Water	2.7	1.9
	#1	Chloroform	46	12.3
Figure 6				
	#1	50% (v/v) isopropyl alcohol	5.7	2.0
	#4	50% (v/v) isopropyl alcohol	0.7	0.4

Figure 7				
	#2	Pentanol	4.0	2.9
	#2	Nonanol	17	4.0

Finally, we determine the values of the molecular displacement distance (λ) of the MKT approach. Using the software, Matlab [50], we iteratively determine the values of λ by solving the discretized equation (3) using the experimental fit of ζ

$$\lambda_{i+1}^2 = \frac{k_B T}{W_a}\left\{ln\left(\frac{\zeta}{\mu}\right) - ln\left(\frac{V_m}{\lambda_i^3}\right)\right\}, \qquad (28)$$

where i is the iteration index. Convergence is rapidly obtained in less than 10 iterations. The displacement distances are listed in the Table 4.

Table 4. Values of the adhesion energy, W_a, coefficient of line friction ζ, molecular displacement distances λ for the different liquids and cubic root of molecular diameter ${V_m}^{1/3}$.

	W_a [mN/m]	ζ [Pa.s]	λ [nm]	${V_m}^{1/3}$ [nm]
Pentanol	54.6	0.12	0.45	0.56
Nonanol	57.1	0.18	0.30	0.66
50% (v/v) Isopropyl Alcohol	62.4	0.12	0.56	0.39
FC-40	31.3	0.22	0.61	0.84
Chloroform	53.1	0.20	0.52	0.51
Water	134.4	0.32	0.51	0.31

Note that, as expected, the displacement distances are in the range of 4 to 7 Angstroms, which is of the order of the cubic root of the molecular volume (V_m): $\lambda^3 \sim V_m$.

Figure 10 shows that the values of the contact-line frictions ζ are in agreement with literature (see Figure SI.3.1)

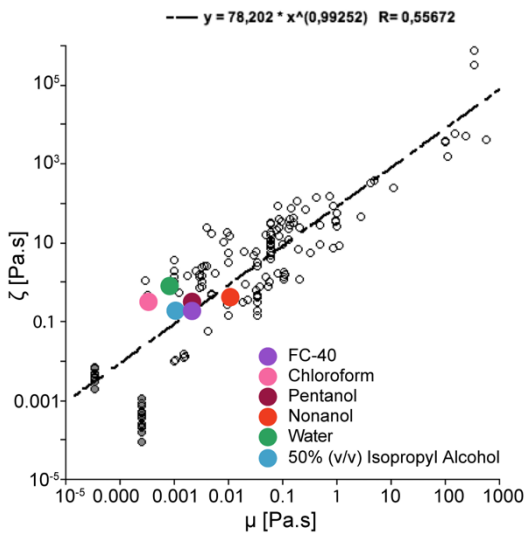

Figure 10. Plot of ζ vs. μ: Comparison of the values collated from the literature (black symbols) and the present study (colored circles) [15]. The literature references are listed in SI.3. Adapted with permission from D. Duvivier, T.D. Blake, J. De Coninck 2013 Toward a predictive theory of wetting dynamics, *Langmuir* **29**(32),10132-10140. Copyright 2023 American Chemical Society.

7. Conclusion

A model for the dynamic contact angle of capillary flows of organic and aqueous liquids in the viscous regime based on the MKT approach has been developed and checked against experiments performed in rectangular open channels made of PMMA.

A closed-form solution is obtained and shows that the real travel distance — using the dynamic contact angle— is equal to the travel distance obtained with the generalized Lucas-Washburn-Rideal law for open-channels minus a correction that correlates the dynamic contact angle to the velocity.

The real velocity of the flow is smaller than the LWR velocity, as reported in the literature for capillary-driven microflows. It is especially seen in the first few centimeters of the channel where the flow is in the early viscous regime.

The MKT model introduces a value of the coefficient of triple line friction that corresponds to local adsorption phenomenon and explains the increase in the contact angle. We reach the same conclusions as Li *et al.* for ionic liquids on fluoropolymer surfaces, that the molecular kinetic model accounts more precisely for dynamic contact angle than hydrodynamic theory [51].

Declaration of competing interest

Ashleigh B. Theberge, Jean Berthier, and Sanitta Thongpang report filing patents through the University of Washington outside this work, and Theberge has received a gift to support research outside the submitted work from Ionis Pharmaceuticals. Sanitta Thongpang has ownership in Salus Discovery, LLC, and Tasso, Inc. Ashleigh B. Theberge and Sanitta Thongpang have ownership in Seabright, LLC, which will advance new tools for diagnostics and clinical research. The terms of this arrangement have been reviewed and approved by the University of Washington in accordance with its policies governing outside work and financial conflicts of interest in research. However, the present publication is not related to these companies. The other authors declare that they have no known competing financial interests or personal relationships that could have appeared to influence the work reported in this paper.

Acknowledgements

We thank Ting Wang for assistance with figure presentation.

This work was funded by National Institutes of Health National Institute of General Medical Sciences grant R35GM128648 (A.B.T.), National Center For Advancing Translational Sciences grant TL1TR002318 (J.C.T.), and the University of Washington. We also acknowledge the M.J. Murdock Diagnostics Foundry for Translational Research. The content is solely the responsibility of the authors and does not necessarily represent the official views of the National Institutes of Health or other funding sources.

References

[1] Chun Huh, L.E. Scriven 1971 Hydrodynamic model of steady movement of a solid / liquid / fluid contact line, Journal of Colloid and Interface Science 35(1), 85-101.
[2] V. Dussan, On the spreading of liquids on solid surfaces: static and dynamic contact lines, Ann. Rev. Fluid Mech., 11, 371, 1979.
[3] T.D. Blake, J.M. Haynes 1973 Contact-angle hysteresis, Progress in Surface and Membrane Science 6, 125-138.
[4] R. Lucas 1918 Ueber das Zeitgesetz des kapillaren Aufstiegs von Flüssigkeiten. Colloid Polym. Sci. 23 (1), 15−22.
[5] E.W. Washburn 1921 The dynamics of capillary flow. Phys. Rev., 17 (3), 273.
[6] E.K. Rideal 1922 On the flow of liquids under capillary pressure, Philos. Mag. 44 (264), 1152−1159.
[7] P-G. De Gennes 1985 Wetting: statics and dynamics**,** Rev. Mod. Phys. 57, 827.
[8] R.G. Cox 1986 The dynamics of the spreading of liquids on a solid surface. Part 1. Viscous flow, J. Fluid Mech., 168,169-194.
[9] O. Voinov 1976 Hydrodynamics of wetting, Fluid Dyn. 11 (5), 714−721.
[10] E.B. Dussan V. 1976 On the difference between a bounding surface and a material surface, J. Fluid Mech. 75 (4), 609−623.
[11] E. Ramé, S. Garoff 1996 Microscopic and macroscopic dynamic interface shapes and the interpretation of dynamic contact angles, J. Colloid Interface Sci. 177 (1), 234−244.
[12] T.D. Blake, J. Haynes 1969 Kinetics of liquid-liquid displacement, J. Colloid Interface Sci. 30 (3), 421−423.
[13] H. Eyring 1935 The Activated Complex in Chemical Reactions*, J. Chem. Phys*. 3 (2), 107–115.

[14] T.D. Blake 2006 The physics of moving wetting lines, J. Colloid Interface Sci. 299 (1), 1−13.
[15] D. Duvivier, T.D. Blake, J. De Coninck 2013 Toward a predictive theory of wetting dynamics, Langmuir 29(32), 10132-10140.
[16] T.D. Blake, J. De Coninck0 2002 The influence of solid−liquid interactions on dynamic wetting, Adv. Colloid Interface Sci. 96(1), 21−36.
[17] G. Martic, F. Gentner, D. Seveno, D. Coulon, J. De Coninck, T. D. Blake 2002 A Molecular Dynamics Simulation of Capillary Imbibition, Langmuir 18, 7971-7976.
[18] P-G. De Gennes, F. Brochart-Wyart, D. Quéré, Capillarity and Wetting Phenomena Drops, Bubbles, Pearls, Waves, Springer, 2004.
[19] R.E. Isele-Holder, A.E. Ismail 2016 Requirements for the formation and shape of microscopic precursors in droplet spreading, Langmuir 32, 4472-4478.
[20] A. Hamraoui, K. Thuresson, T. Nylander, and V. Yaminsky 2000 Can a dynamic contact angle be understood in terms of a friction coefficient? Journal of Colloid and Interface Science 226**,** 199–204.
[21] P. Wu, A. Nikolov, D. Wasan 2017 Capillary dynamics driven by molecular self-layering, Adv. Colloid Interface Sci. 243, 114−120.
[22] P. Wu, A.D. Nikolov, and D.T. Wasan 2017 Capillary rise: Validity of the dynamic contact angle models, Langmuir 33, 7862−7872.
[23] R.L. Hoffman 1975 A study of the advancing interface. I. Interface shape in liquid—gas systems, J. Colloid Interface Sci. 150 (2), 228−241.
[24] L.H. Tanner 1979 The spreading of silicone oil drops on horizontal surfaces, Phys. D: Appl. Phys., 12(9), 1473-1485.
[25] T.S. Jiang, S.G. Oh, J.C. Slattery 1979 Corrections for dynamic contact angle, J. Colloid Interface Sc. 69(1), 74-77.
[26] M. Bracke, E De Voeght, and P. Joos 1989 The kinetics of wetting: the dynamic contact angle, Progr Colloid Polym Sci 79, 142-149.
[27] P. Joos, P. Vanremoortere, M. Bracke 1990 The kinetics of wetting in a capillary, J. Colloid Interface Sci. 136 (1), 189−197.
[28] J.E. Seebergh, J.C. Berg 1992 Dynamic wetting in the low capillary number regime, Chem. Eng. Sc. 47 (17), 4455.
[29] B.P. Casavant, E. Berthier, A.B. Theberge, J. Berthier, S.I. Montanez-Sauria, L.L. Bischel, K.A. Brakke, C.J. Hedman, W. Bushman, N.P. Keller, D.J. Beebe 2013 Suspended microfluidics PNAS 110(35), 10111-10116.
[30] J. Berthier, D. Gosselin, E. Berthier 2015 A generalization of the Lucas–Washburn–Rideal law to composite microchannels of arbitrary cross section, Microfluidics and Nanofluidics 19, 497-507.
[31] J. Berthier, K.A; Brakke, E. Berthier, Open-Microfluidics, Scrivener-Wiley Publishing, 2016.
[32] E. Berthier, A.M. Dostie U. N. Lee, J. Berthier, and A.B. Theberge, 2019 Open microfluidic capillary systems, Anal. Chem. 91, 8739−8750.
[33] N.M. Oliveira, S. Vilabril, M.B. Oliveira, R.L. Reis, J.F. Mano 2019 Recent advances on open fluidic systems for biomedical applications: A review, Materials Science and Engineering: C 97, 851-863.
[34] B. Lee, S. Kim, J. Ko, S-R. Lee, Y. Kim, S. Park, J. Kim, S. Hyung, H-Y. Kim, N.L. Jeon 2022 3D micromesh-based hybrid bioprinting: multidimensional liquid patterning for 3D microtissue engineering, Asia Material 14, 6-16.
[35] M.M. Weislogel, J.C. Graf, A.P. Wollman, C.C. Turner, K.J.T. Cardin, L.J. Torres, J.E. Goodman and J.C. Buchli 2022 How advances in low-g plumbing enable space exploration, NPJ Microgravity 8, 16-27.
[36] P. Concus and R. Finn 1969 On the behavior of a capillary surface in a wedge, PNAS 63 (2), 292–299.
[37] J. Berthier, A.B. Theberge, E. Berthier, Open-channel microfluidics, IOP Publishing, 2019.
[38] F.F. Ouali, G. McHale, H. Javed, C. Trabi, N.J. Shirtcliffe, M.I. Newton 2013 Wetting considerations in capillary rise and imbibition in closed square tubes and open rectangular cross-section channels, Microfluidics Nanofluidics 15 (3) 309–326.
[39] R.K. Lade, Jr., E.J. Hippchen, C.W. Macosko, L.F. Francis 2017 Dynamics of capillary-driven flow in 3D printed open microchannels, Langmuir 33, 2949−2964.
[40] G.B. Abadi & M. Bahrami 2022 The effect of surface roughness on capillary rise in micro-grooves Scientific Reports 12, 14867.
[41] D. Gloss, H. Herwig 2012 Wall roughness in laminar flows: an often ignored though significant issue, Exp. In Fluids 49(2), 461-470.
[42] A. Vesel, M. Mozetic 2012 Surface modification and ageing of PMMA polymer by oxygen plasma treatment, Vacuum 86, 634-637.

[43] A. Sikora, D. Czylkowski, B. Hrycak, M. Moczała-Dusanowska, M. Łapiński, M. Dors, M. Jasiński 2021 Surface modification of PMMA polymer and its composites with PC61BM fullerene derivative using an atmospheric pressure microwave argon plasma sheet, Scientific Reports, 11, 9270.
[44] S. Kim, P.A. Thiessen, E.E. Bolton, J. Chen, G. Fu, A. Gindulyte, L. Han, J. He, S. He, B.A. Shoemaker, J. Wang, B. Yu, J. Zhang, S.H. Bryant 2016 PubChem Substance and Compound Databases. Nucleic Acids Res., 44, D1202.
[45] A.A. Mohammad, K.H.A.E. Alkhaldi, M.S. AlTuwaim, A.S. Al-Jimaz, A. S. 2014 Effect of Temperature and Chain Length on the Viscosity and Surface Tension of Binary Systems of N, N-Dimethylformamide with 1-Octanol, 1-Nonanol and 1-Decanol. J. Chem., Thermodyn. 74, 7–15.
[46] J.J. Lee, J. Berthier, A.B. Theberge, E. Berthier 2019 Capillary flow in open microgrooves: bifurcations and networks, Langmuir 35(32), 10667-10675.
[47] J. Berthier, K.A. Brakke, E. Berthier 2014 A general condition for spontaneous capillary flow in uniform cross-section microchannels, Microfluidics Nanofluidics 16, 779–785.
[48] L-H. Chang, S. Kumar, Capillary filling in open rectangular microchannels with a spatially varying contact angle, Langmuir December 3, 2023.
[49] D. Quéré 2007 Inertial capillarity, Europhysics Letters 39(5), 533.
[50] MATLAB, https://www.mathworks.com/
[51] H. Li, R. Sedev, J. Ralston 2011Dynamic wetting of a fluoropolymer surface by ionic liquids, Phys. Chem. Chem. Phys.13, 3952–3959